Applied Energy 195 (2017) 877–889

Contents lists available at ScienceDirect

Applied Energy

journal homepage: www.elsevier.com/locate/apenergy

Dynamic modeling of a sensible thermal energy storage tank with an immersed coil heat exchanger under three operation modes

Austin L. Nash [a], Apurva Badithela [b], Neera Jain [a,*]

[a] Purdue University, West Lafayette, IN 47907, United States
[b] University of Minnesota, Minneapolis, MN 55455, United States

HIGHLIGHTS

- A control-oriented dynamic model of a thermal energy storage tank is proposed.
- The dynamic tank model is spatially discretized into *n* nodes.
- Simplifying assumptions enable an accurate yet zero-order immersed coil HX model.
- The model is experimentally tuned and validated.
- The model is well-suited for advanced control design and real-time simulation.

ARTICLE INFO

Article history:
Received 21 December 2016
Received in revised form 20 February 2017
Accepted 19 March 2017
Available online 31 March 2017

Keywords:
Dynamic modeling
Control-oriented modeling
Thermal energy storage
Immersed heat exchanger
Hot water storage tank
Waste heat recovery
Demand response

ABSTRACT

In this paper we consider control-oriented modeling of a sensible thermal energy storage (TES) tank with a helical immersed heat exchanger (IHX) coil. A key focus of the modeling approach is to minimize the number of dynamic states required to adequately describe the system dynamics. The resulting model is well-suited for model-based control design, real-time simulation, and hardware-in-the-loop testing aimed at intelligent operation of TES systems. We use a discretized approach to model the temperature dynamics of the water within the storage tank. We use a quasi-steady approach to model the IHX coil dynamics, thereby limiting computational complexity. In simulation, the model runs up to 1200× faster than real-time. A simulated case study of model-based feedback control demonstrates the utility of the modeling approach. The model contains four tuning parameters that are empirically determined using experimental data collected from a commercially available domestic hot water storage tank. The model is then validated, both temporally and spatially, against data collected during the simultaneous charge/discharge mode. Finally, we quantify the trade-off between model fidelity and increased control volume discretization, showing that a 60 node model yields a RMSE value under 4.5%.

1. Introduction

In U.S. industrial processes alone, 20–50% of the energy input is lost as waste heat [1,2]; across all sectors, a total of 61% of energy was wasted in 2015 [3]. Without the ability to capture and utilize waste heat across a wide range of sectors, an increase in the total amount of energy - both from fossil fuels and renewables - will be needed to meet future energy demand [4]. Current efforts to recover waste heat target mostly large-scale, centralized applications (such as cogeneration plants for large campuses or industrial complexes) where the dynamics are sufficiently slow to enable simple control logic to guide system operation [5,6]. The majority of these applications utilize "heat-to-power", or direct conversion of waste heat to electricity. This electricity is then delivered immediately to the grid or another subsystem which can use it without any storage mechanism in between [7]. Such heat-to-power systems generally require high-temperature waste heat. However, more than 80% of waste heat in the industrial sector alone is actually low- or medium-temperature waste heat [1,8], and the figure is closer to 85% across all sectors in the U.S. [9]. Therefore, a significant amount of work potential remains unutilized.

One challenge that arises in waste heat recovery scenarios is that the availability of thermal energy may not be synchronized with the demand. Fortunately, thermal energy storage (TES) systems can be used to temporally decouple recovery from utilization as shown in Fig. 1. However, this requires intelligent management

* Corresponding author.
E-mail addresses: nash@purdue.edu (A.L. Nash), badit001@umn.edu (A. Badithela), neerajain@purdue.edu (N. Jain).

http://dx.doi.org/10.1016/j.apenergy.2017.03.092
0306-2619/

Nomenclature

Δ	internal heat transfer scaling parameter	$j-1$	represents node above node j
$\dot{m}_c$	mass flow rate of IHX coil fluid	k	internal node interaction heat transfer coefficient
$\dot{m}_{cw}$	mass flow rate of inlet domestic cold water	k_w	lumped heat transfer coefficient for losses across walls
$\dot{m}_t$	discharge mass flow rate through tank	m	mass of node
$\dot{Q}_{coil}$	heat transfer rate due to IHX coil	s_1	discharge fluid correction factor
$\dot{Q}_{j+1}$	heat transfer rate between nodes j and $j+1$	T	temperature
$\dot{Q}_{j-1}$	heat transfer rate between nodes j and $j-1$	t	time
$\dot{Q}_{wall}$	heat transfer rate for losses to surroundings	T_{cw}	domestic cold water temperature
A	cross-sectional area of node control volume	T_{en}	IHX coil fluid inlet temperature
A_w	wall contact surface area	T_{ex}	IHX coil fluid outlet temperature
c_v	specific heat capacity of water	w_t	tank wall thickness
j	current node in iterative energy equations	z	vertical height variable with respect to tank bottom
$j+1$	represents node below node j		

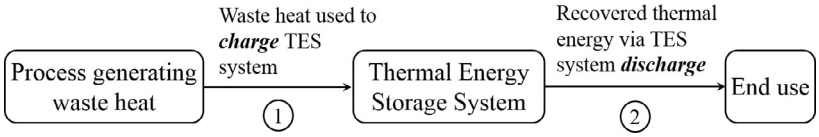

Fig. 1. Conceptual flow chart of waste heat recovery. Thermal energy storage systems can be used to temporally decouple processes 1 and 2.

of TES system operation. In order to implement real-time control of a TES system, and thus modulate the charging and discharging rates according to predictions of waste heat availability or demand response, a control-oriented dynamic model of the TES system is required.

A typical control-oriented model has the following characteristics:

1. it is computationally inexpensive
2. it is parameterized with respect to key system control variables.

Such a model can facilitate advanced control of the TES system in order to optimize its performance. In the context of low- to medium-temperature waste heat recovery, one application of waste heat recovery integrated with thermal energy storage is a PEM (proton exchange membrane) fuel cell micro-combined heat and power (micro-CHP) system wherein the fuel cell is used to produce electricity. A coolant, typically deionized (DI) water, absorbs heat from the fuel cell in order to keep it within operational temperature constraints. The DI water then rejects the heat it has absorbed to a TES system such as a hot water storage tank. Since the DI water cannot become contaminated, it must remain decoupled from the thermal storage medium. This is made possible through the use of a sensible (liquid) thermal energy storage tank with an immersed heat exchanger (IHX) coil. Unfortunately, most existing models of liquid storage tanks, both with and without IHX coils, are not control-oriented. Furthermore, existing control-oriented models [10,11] have primarily been aimed at storage tanks without IHX coils.

The contribution of this work is an experimentally tested control-oriented model of a sensible thermal energy storage tank with an immersed coil heat exchanger. A discretized modeling approach for the storage tank is coupled with a quasi-steady IHX coil model. The latter leverages key simplifications in order to capture the charging dynamics of the overall system with fewer dynamic states. The resulting model maintains an almost-linear structure that is particularly well-suited for model-based control design. The derived model is also suitable for real-time simulation and hardware-in-the-loop testing.

The rest of the paper is organized as follows. In Section 2, we present a background of the various models available in the literature for hot water storage tanks. We derive our control-oriented model in Section 3 and present model tuning and experimental validation results in Section 4. Conclusions are summarized in Section 5.

2. Background

2.1. Modeling approaches for hot water storage tank dynamics

The governing dynamic equations of hot water storage tanks are multidimensional partial differential equations that describe conservation of mass, momentum, and energy. Numerous authors have derived higher order two-dimensional and three-dimensional numerical and CFD (computational fluid dynamics) models to simulate the dynamics and performance of various storage tank configurations [12–18]. These types of models are useful for offline simulations aimed at making key design decisions such as optimal placement of flow valves. However, these models are too computationally expensive to be used for real-time simulation or model-based control design.

Alternatively, many studies utilize one-dimensional (1D) models which apply spatial discretization techniques to the storage tank with lumped parameter assumptions made for each control volume, or node [19,16,20,10,21,11]. These models eliminate the need for a momentum balance. While the 1D models are more computationally efficient than higher-order models, complexities which hinder real-time control still exist. For example, 1D models require a method of accounting for temperature inversion. Temperature inversion is a phenomenon that occurs when high temperature water exists below low temperature water. One-dimensional models inherently do not account for the buoyancy that causes the warmer, less dense water to rise within the tank. Accounting for temperature inversion in 1D models usually involves a mixing algorithm wherein, at the end of each time step, nodes affected by inversion are mixed, or combined, to obtain one node at a single mean temperature value [20]. Another method

involves simply reordering control volumes at the end of each time step such that high temperature control volumes are located above low temperature control volumes. These methods are difficult to utilize in real-time simulations due to the computations that must be completed after each time step.

Some researchers have recently developed control-oriented 1D tank models which aim to accurately capture dominant dynamics in a less computationally-expensive way. Powell, et al. [10] employ an adaptive-grid model in which the top and bottom nodes of the tank are allowed to vary in size in order to avoid over-discretizing the model in isothermal regions. The authors also introduce an alternative scheme to account for temperature inversion wherein high heat transfer coefficients are used to model heat transfer between adjacent nodes experiencing temperature inversion. This allows temperature inversion to be accounted for in such a way that facilitates real-time simulation [10]. Additionally, Baeten, et al. present a 1D model in which they incorporate 3D mixing effects through the use of nondimensional inflow and outflow parameters [11]. These types of models are crucial for model-based control design of TES systems. *However, these existing low-order models do not incorporate the existence of an immersed coil heat exchanger within the tank, a configuration which requires modeling of additional dynamics due to the presence of a heating coil.*

2.2. Modeling storage tanks with immersed coil heat exchangers

Hot water storage tanks exist in many configurations, several of which are shown in Fig. 2. Models are often developed to simulate cases where both sink and source mass flow loops exist (Fig. 2a) [20,10]. Other models attempt to predict dynamics for tanks with mantle heat exchangers (Fig. 2b) [22–24]. In this work, the storage tank contains an IHX coil (Fig. 2c). From a modeling perspective, the IHX architecture permits several simplifying assumptions to be made which help reduce overall model complexity, thereby making the model useful in real-time control. For example, the existence of a single flow loop allows the assumption that mixing effects due to downward flow can be assumed negligible since incoming flow exists only at the bottom of the tank.

Most efforts at modeling storage tanks with IHX coils involve a level of complexity that hinders computational efficiency. This complexity arises from two main sources. The first is the addition of a second set of discretized dynamics. For example, in [25], the authors present a method of modeling the heat exchanger by discretizing it into a set of control volumes with transient energy dynamics. While accurate, this method increases the number of dynamic states needed to describe the storage tank dynamics, thereby increasing computational complexity.

The second type of complexity in modeling IHX coils involves using steady-state conductive and convective heat transfer correlations to capture heat transfer between the coil and the storage medium. These methods typically aim to derive an overall heat transfer coefficient for the coil or a fluid temperature profile for the fluid within the IHX coil. This usually involves many table look-ups and equations to calculate nondimensional variables such as the Nusselt number, Prandtl number, and Reynolds number. In [26], the authors use heat transfer correlations to characterize the performance of a load-side immersed coil heat exchanger. Logie and Frank use a coil discretization scheme with a Newton-Raphson method to iteratively solve for an average IHX wall temperature for each coil control volume [27]. In [28,29], the authors expand upon previous work by incorporating an IHX model using steady-state heat transfer correlations. In [30], the authors confine the IHX coils to a single node and use convective heat transfer correlations and an experimentally-tuned heat transfer correction coefficient to incorporate the coil dynamics. Additional research has focused more generally on modeling the dynamics of submerged, coiled heat exchangers [31–37].

All of these models provide the ability to simulate the effects of an IHX coil on storage tank performance. However, there are two key aspects that hinder their use in control-oriented modeling:

1. the heat transfer correlations add computational complexity, and
2. they are not easily parameterized with respect to the mass flow rate through the coil, the key control variable in the context of this work.

For use in real-time control, the overall dynamic model must be in a form that is well-suited for model-based control design. The model should be an explicit function of the main control variables (easily parameterized with respect to the main control variables) in order to capture the relationship between the control inputs and system performance. Therefore, in this paper, we unite control-oriented sensible thermal energy storage tank modeling with control-oriented modeling of an immersed coil heat exchanger. In the following section, we develop a quasi-steady model of the immersed coil dynamics which is independent of heat transfer correlations and readily parameterized with respect to the flow rate of waste heat fluid through the IHX coil. We also describe simple strategies that serve to account for effects of mixing and buoyancy. We present a simulated case study to show how the resulting model can be used in real-time control. The dynamic model is then tuned and validated on an experimental cylindrical hot water storage tank with a helical immersed coil heat exchanger.

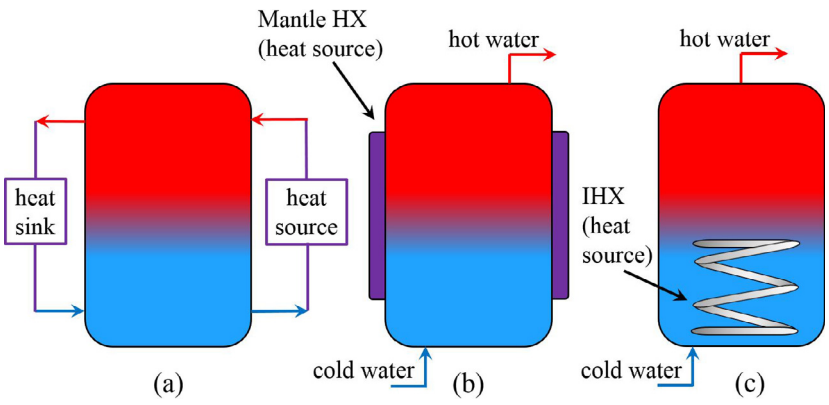

Fig. 2. Various configurations of hot water storage tanks. (a) Storage tank with dual heat sink and heat source mass flow loops. (b) Storage tank with mantle heat exchanger in contact with tank wall. (c) Storage tank with an IHX coil.

3. Switched-mode model derivation

In this section, we derive a control-oriented model for a cylindrical sensible thermal energy storage tank with a helical immersed coil heat exchanger. First, we describe the storage tank under consideration and its modes of operation. We then derive a dynamic model for the storage tank itself, followed by a quasi-steady approximation of the dynamics for the IHX coil. We then present two simulated case studies. The first case study illustrates the model's ability to replicate the dynamics acting during different modes of system operation. The second case study demonstrates how the model can be used to design a model-based feedback controller to meet load demand during modes involving discharge.

3.1. Storage tank modes of operation

A schematic of the cylindrical thermal energy storage tank with an IHX is shown in Fig. 3.

Fluid carrying waste heat, from here forward to be called waste heat fluid, at a temperature T_{en} enters an IHX coil situated at the lower portion of the tank. The waste heat fluid is then pumped vertically through the coil until it exits the tank at T_{ex}. Heat is transferred from the waste heat fluid flowing through the coil to the colder fluid in the tank. We define three different modes of operation for the system.

1. *Charging*: The heat addition mode, or the mode during which waste heat fluid is pumped through the coil in order to heat the colder fluid in the tank. The thermocline location is static and lies at the height where hot waste heat fluid enters the tank.
2. *Discharging*: The heat rejection mode, or the mode during which hot fluid is pumped out of the tank and replaced with cold fluid. The hot fluid is removed from the tank at a flow rate $\dot{m}_t$ which acts as a disturbance on the system. Moreover, the fluid in the tank is replenished at a flow rate of $\dot{m}_{cw}$ which enters at the bottom of the tank. During this mode, the thermocline moves vertically through the tank.
3. *Simultaneous charging/discharging*: Heat is both absorbed by the tank from the IHX and removed from the tank via the discharge flow. During this mode, the thermocline moves vertically through the tank.

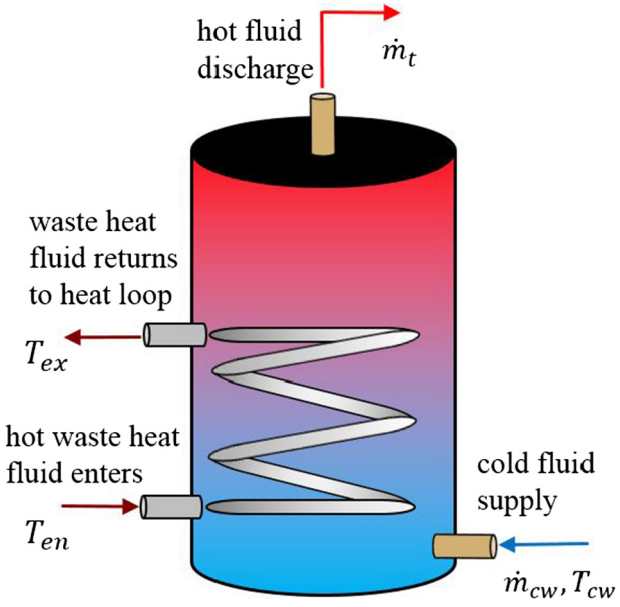

Fig. 3. Schematic of storage tank and IHX.

3.2. Multinode model of sensible TES tank

To model the temperature dynamics of the fluid within the storage tank, we use a multinode model similar to that used in [20,10]. The tank is discretized vertically into n nodes, with the top node defined as node one. A schematic of a discretized control volume is shown in Fig. 4. Within each discretized node, we make a lumped-parameter assumption with respect to the temperature, density, and specific heat of the fluid contained within the node. In other words, density and specific heat are allowed to vary between nodes as a function of node temperature, but are treated as constant (spatially) within a single node.

Each node is allowed to exchange heat with its surroundings in several ways. Nodes can absorb heat from the coil, $\dot{Q}_{coil}$, and reject heat to the tank wall and the ambient through the lumped heat transfer rate term $\dot{Q}_{wall}$. Additionally, each node is allowed to exchange heat with its bordering nodes, modeled separately as $\dot{Q}_{j+1}$ and $\dot{Q}_{j-1}$. While in discharge mode, we introduce the assumption that fluid only flows upward through each control volume. Each node is assumed to remain in steady-state with respect to mass flow rate, and the bottom node is always sized such that it contains the cold fluid inlet flow valve. Therefore, we assume that mass does not move downward within the tank.

Conservation of energy is used to derive a system of n ordinary differential equations that can be solved numerically, yielding the temperature stratification in the storage tank as a function of time. For the jth node, we define the energy balance equation to be

$$m_j c_{vj} \frac{dT_j}{dt} = \dot{Q}_{coil,j} - \dot{Q}_{wall,j} + \dot{Q}_{j+1} - \dot{Q}_{j-1} + s_1 \dot{m}_t c_{vj} (T_{j+1} - T_j). \quad (1)$$

Because there exists a single flow loop, and because the inlet and outlet flow valves are positioned at the bottom and top of the tank, respectively, we assume the effects of fluid mixing due to discharge flow to be fairly minimal. We introduce a scaling variable s_1 as a tunable parameter to represent the average interface temperature between adjacent nodes. The scaling variable is bounded by $0 \leqslant s_1 \leqslant 1$ and is taken to be the same for all nodes. Heat transfer due to interactions between the storage tank fluid and both the tank walls and the ambient environment are lumped into a single heat transfer rate term, given by

$$\dot{Q}_{wall,j} = \frac{k_w A_{w,j}}{w_t} (T_j - T_0), \quad (2)$$

where k_w is an empirically identified lumped heat transfer coefficient, w_t is the approximate wall thickness, T_0 is the temperature of the ambient environment, and A_w is the wall surface area in contact with each respective node. The internal heat transfer rate terms $\dot{Q}_{j-1}$ and $\dot{Q}_{j+1}$ are solved using a finite difference scheme with a temperature inversion correction method adapted from [10]. Fig. 5 illustrates the process.

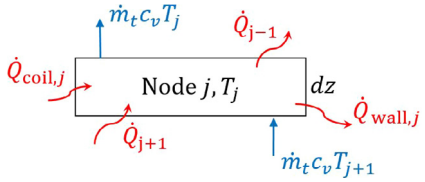

Fig. 4. A discretized control volume.

The expressions describing heat transfer due to nodal interactions are given by

$$\dot{Q}_{j-1} = -k_{j-1}A\frac{T_{j-1}-T_j}{z_{j-1}-z_j}, \tag{3}$$

$$\dot{Q}_{j+1} = -k_{j+1}A\frac{T_j-T_{j+1}}{z_j-z_{j+1}}. \tag{4}$$

At any point during a simulation, if the temperature of node j is either lower than the temperature of the node below it, or higher than the temperature of the node above it, the k_{j-1} and k_{j+1} terms are increased by several orders of magnitude in order to force heat to be transferred upward, thereby addressing the temperature inversion problem [10]. The algorithm for the variation of the coefficients is given by Eqns. (5) and (6),

$$k_{j-1} = \begin{cases} k_{j-1}\Delta|T_j - T_{j-1}|, & \text{if } T_j > T_{j-1} \\ k_{j-1}, & \text{otherwise} \end{cases} \tag{5}$$

$$k_{j+1} = \begin{cases} k_{j+1}\Delta|T_j - T_{j+1}|, & \text{if } T_j < T_{j+1} \\ k_{j+1}, & \text{otherwise} \end{cases}, \tag{6}$$

where Δ is a tunable parameter whose magnitude is several orders higher than the magnitude of the k term itself. Because the IHX is placed near the bottom of the tank, the tank is subject to temperature inversion during any mode involving charge. As the temperature inversion occurs, some heat transfer coefficients increase drastically in magnitude whereas other heat transfer coefficients remain constant. Consequently, the temperatures of some nodes change much faster than others, resulting in a stiff system. Therefore, we modified this temperature inversion scheme by introducing two magnitude terms $|T_j - T_{j-1}|$ and $|T_j - T_{j+1}|$ to obtain dynamic coefficients that serve to limit adverse computational effects due to temperature inversion. If minimal temperature inversion exists, the resulting dynamic heat transfer coefficients take on smaller magnitudes, thereby imposing less numerical burden on the model. In other words, the level of compensation for temperature inversion is proportional to the difference in temperature between adjacent nodes.

3.3. Modeling heat transfer due to an immersed coil heat exchanger

In an effort to minimize the number of dynamic states in the model across all operation modes, we pursue a quasi-steady approach to modeling the heat transfer between the IHX coil and the fluid within the tank. The quasi-steady modeling strategy is based upon the idealized assumption that the effectiveness of the immersed heat exchanger is one. Therefore, at any time t, based on the assumption above, we take the value of T_{ex} to be equal to the temperature of the fluid of the surrounding tank node. The merits of this assumption will be demonstrated with a model-based feedback control case study in Section 3.5.

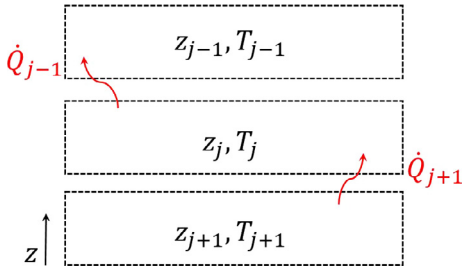

Fig. 5. Finite difference scheme for discretized node.

The fluid entering the IHX coil is at a known temperature, T_{en}. To calculate the heat transfer rate between the coil and the tank node(s) within the coil region, we treat the immersed coil as a separate subsystem acting at steady-state with known inlet (T_{en}) and outlet (T_{ex}) fluid temperatures. Moreover, the thermocline is static during pure charge mode (when no discharge occurs); it consistently lies at the vertical height of the hot waste heat fluid inlet valve. High discretization is unnecessary to get an accurate temperature profile; in fact, high discretization impinges on the model's computational efficiency due to the high degree of temperature inversion within the storage tank. Therefore, a two-node model is used during pure charge mode wherein the bottom node represents the cold section below the bottom of the IHX coil region and the top node represents the hot section in and above the IHX coil region. The hot section is heated uniformly as the charge progresses, and all of the heat transferred into the storage tank by the IHX coil is confined to the top discretized node. Fig. 6 illustrates this.

The tank is assumed to be ideally stratified at the coil inlet height. The heat transferred into the tank in pure charge mode is then calculated as

$$\dot{Q}_{coil} = \dot{m}_c c_{v,1}(T_{en} - T_{ex}), \tag{7}$$

where $c_{v,1}$ is calculated according to the current top node temperature.

Conversely, the thermocline location is dynamic during simultaneous charge/discharge mode. Therefore, a much finer discretization is necessary to capture the thermal dynamics in the storage tank. During simultaneous charge/discharge mode, logic is used to determine whether each node is within the coil region which in turn dictates whether or not there is heat transfer between the coil and that particular node. A zero-order (algebraic) modeling scheme is then applied to characterize all nodal coil heat transfer rates.

To calculate the heat transfer rate between the coil and the tank nodes within the coil region, we employ a quadratic coil fluid temperature reduction profile from the tank coil inlet to the tank coil outlet. Any node determined to be within the coil region in the storage tank is assumed to contain a corresponding discretized slice of the helical coil. This concept is further illustrated in Fig. 7.

The same assumptions apply for T_{en} and T_{ex}; the value of T_{en} is known and T_{ex} is taken to be equal to the temperature of the node

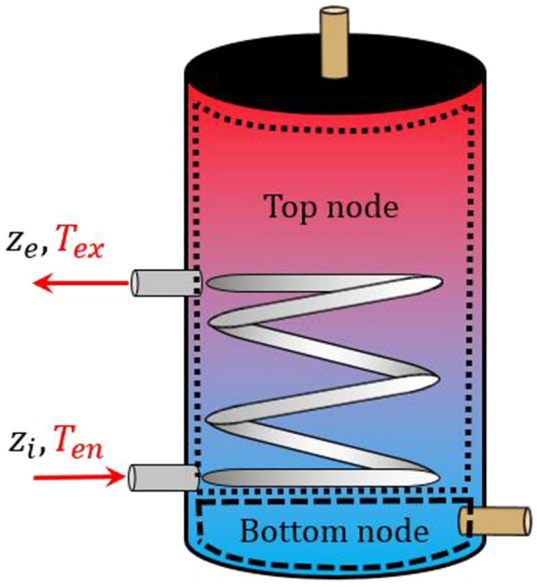

Fig. 6. Schematic of discretization in pure charge mode.

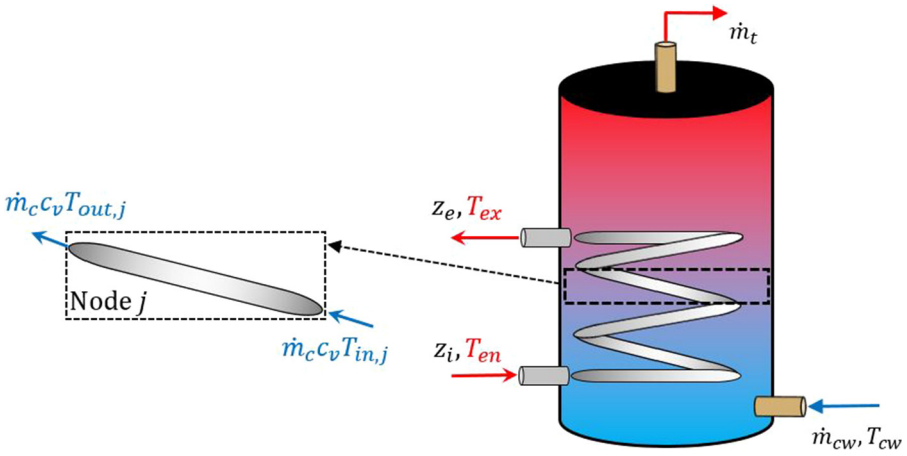

Fig. 7. Schematic for calculating heat transfer rates due to the immersed coil.

containing the hot waste heat fluid outlet valve. We empirically observed that the *fluid in the storage tank* (within the coil region) experiences a quadratic increase in temperature as a charge progresses. We then assume that the *fluid in the IHX coil* decreases according to a similar quadratic profile. As such, we calculate the *coil fluid* inlet and outlet temperatures for each *j*th node in the coil region according to a quadratic temperature reduction curve between T_{en} to T_{ex} with respect to vertical node height z. A user-defined third point is chosen to create the quadratic polynomial. This is shown in Fig. 8. Coil heat transfer rate terms for nodes outside the coil region are assigned a zero value.

The resulting profile allows a completely algebraic characterization of the heat transfer from the IHX to the tank fluid. Each nodal heat transfer rate is calculated according to

$$\dot{Q}_{coil,j} = \dot{m}_c c_{v,j}\left(T_{in,j} - T_{out,j}\right). \tag{8}$$

As discussed, the IHX coil model assumes that the hot fluid always exits the coil at the same temperature as the fluid in the surrounding storage tank node. While this assumption may not be appropriate for some types of analysis, we will show its usefulness in the context of the control-oriented modeling in this work. This method of calculating the heat transfer rate from the IHX to the tank is computationally-inexpensive because (1) no heat transfer correlations are needed and (2) it does not add any dynamic states into the overall model. More importantly, each dynamic state which is subject to heat transfer from the coil is conveniently parameterized with respect to the main control input variable $\dot{m}_c$. In other words, $\dot{m}_c$ is responsible for driving the coil heat transfer rate. This feature will be instrumental in using the model for real-time control of the storage tank.

To illustrate the simplicity of the dynamic model, note that by taking the modeling approach described in this section, we can conveniently formulate a matrix-vector model of the system dynamics as shown in Eq. (9). This system description lends itself well to both real-time control and optimization. A simple control example will further illustrate this point in Section 3.5.

For all modes of operation, the model is simulated using a stiff Runge-Kutta ODE solver on a computer with a 3.3 GHz processor. The user defines the dimensions of the storage tank, along with the location of all inlet/outlet valves. During pure charge mode, the two-node model is used. However, for pure discharge or simultaneous charge/discharge mode, the user specifies the number of nodes desired. The model is then discretized accordingly. To demonstrate the computational value of the model, we evaluate the computational speed of the simulation model with respect to real-time system operation for each mode as shown in Table 1.

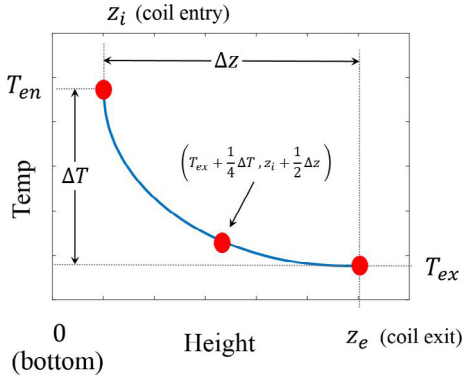

Fig. 8. Depiction of quadratic coil waste heat fluid temperature reduction scheme. The waste heat fluid enters with temperature T_{en} at height z_i before exiting with temperature T_{ex} at height z_e. A quadratic curve fit is generated and used to estimate values of $T_{in,j}$ and $T_{out,j}$ for each node within the tank's coil region.

The model is the most computationally expensive in simultaneous charge/discharge mode due to the temperature inversion scheme combined with the higher discretization. Nevertheless, even with temperature inversion, the simultaneous charge/discharge model runs approximately 200 times faster than real-time. In both charge mode and discharge mode, little to no temperature inversion exists, and the model is virtually unlimited in terms of speed.

$$\begin{Bmatrix} m_1 c_v \frac{dT_1}{dt} \\ m_2 c_v \frac{dT_2}{dt} \\ m_3 c_v \frac{dT_3}{dt} \\ \vdots \\ m_{n-1} c_v \frac{dT_{n-1}}{dt} \\ m_n c_v \frac{dT_n}{dt} \end{Bmatrix} = \begin{bmatrix} \alpha & \beta & 0 & \cdots & & \\ \gamma & \alpha & \beta & 0 & \cdots & \\ 0 & \gamma & \alpha & \beta & 0 & \cdots \\ & & & \vdots & & \\ 0 & \cdots & & \gamma & \alpha & \beta \\ 0 & \cdots & & & \gamma & \alpha \end{bmatrix} \begin{Bmatrix} T_1 \\ T_2 \\ T_3 \\ \vdots \\ T_{n-1} \\ T_n \end{Bmatrix} + \begin{bmatrix} \zeta \\ \vdots \\ 0 \end{bmatrix} \dot{m}_c + \begin{bmatrix} \eta & \delta \\ \vdots & \vdots \\ & \\ & \\ 0 & \end{bmatrix} \begin{Bmatrix} \dot{m}_t \\ T_0 \end{Bmatrix}$$

$$\alpha = -\left(\frac{k_{j-1}A}{\Delta z_j} + \frac{k_{j+1}A}{\Delta z_j} + \frac{k_w A_w}{w_t}\right), \quad \beta = \frac{k_{j+1}A}{\Delta z_j}, \quad \gamma = \frac{k_{j-1}A}{\Delta z_j},$$

$$\delta = \frac{k_w A_w}{w_t}, \quad \zeta = c_v\left(T_{in,j} - T_{out,j}\right), \quad \eta = s_1 c_v\left(T_{j+1} - T_j\right) \tag{9}$$

3.4. Simulated case study of system dynamics

Here we present a simulated case study demonstrating the model's ability to capture tank temperature evolution during simultaneous charge/discharge mode. The tank is initially charged for two hours. During this time, waste heat water from an inte-

Table 1
Computational speed of the simulation model. The simulation speed column represents the speed of each simulation as compared to real-time.

Mode	Simulation speed
Charge	1250×
Discharge	800×
Simultaneous charge/discharge	200×

Table 2
Baseline values used for the hot water storage tank in the simulated case study.

Parameter	Value	Parameter	Value
Tank height	1.3 m	Coil volumetric flow rate	$3.34 \cdot 10^{-5}$ m^3/s
Tank diameter	0.4 m	Tank volumetric flow rate	$1.26 \cdot 10^{-4}$ m^3/s
Tank initial temperature	20 °C	Number of nodes	60
T_0	20 °C	z_i	0.15 m
T_{en}	45 °C	z_e	0.58 m
T_{cw}	20 °C	w_t	0.051 m
k_w	0.25 W mK^{-1}	k	1 W mK^{-1}
Δ	100,000	s_1	0.92

grated power generation system flows through the coil, thereby exchanging heat with the tank. At the two hour mark, the tank enters the simultaneous charging/discharging mode in which hot water is removed from the tank at a specified flow rate $\dot{m}_t$ while heat continues to be added to the system through the IHX. Table 2 gives the parameters used in the simulation. The temperature evolution of the thermal stratification for this mode, over a period of 30 min, is shown in Fig. 9.

In Fig. 9a, the charge/discharge has been ongoing for ten minutes. A portion of the hot water above the coil region has exited the tank and been replenished with the cold water supply. However, the waste heat water inside the coil continues to heat the cold water as it is drawn upwards through the tank. In Fig. 9b, it is clear that the hottest water in the tank, which was located above the coil at a temperature near 40 °C, has been removed from the tank. Finally, in Fig. 9c, all of the water above the coil region is at a temperature below 30 °C. At this point, the tank contains an isothermal temperature section above the coil region; water being discharged from the tank is heated from the cold water supply temperature of 20 °C to about 27 °C before it rises above the IHX coil and eventually exits the tank.

3.5. Simulated case study of model-based feedback control

Throughout Section 3 we have derived a control-oriented model of the storage tank and IHX coil dynamics. We have also detailed several simplifying assumptions, namely with respect to the IHX coil heat transfer. Now, we show how these assumptions lead to a model structure that can easily be used for feedback control design. As illustrated in the previous case study, discharge of water from the top node can be viewed as a disturbance acting to deplete the storage tank of its charge and meet some load demand. In order to reject this disturbance, or in other words, ensure that the load demand is met, the coil flow rate, $\dot{m}_c$, can be modulated accordingly. The following case study will illustrate this in detail.

The schematic shown in Fig. 10 defines the key variables and control volumes in this case study. For simplicity, we confine the IHX coil to the bottom node so that the tank is always under temperature inversion while the storage tank is charging. The coil exit temperature, T_{ex}, is assumed to be equal to the temperature of the bottom node, T_2, at any time t. For this example, we assume constant density and specific heat. In general, however, they can be left as time-varying. In accordance with Eq. (9), the governing energy balances for each node can be represented by Eq. (10).

$$\begin{Bmatrix} m_1 c_v \frac{dT_1}{dt} \\ m_2 c_v \frac{dT_2}{dt} \end{Bmatrix} = \begin{bmatrix} -\left(\frac{kA}{h_1} + \frac{k_w A_w}{w_t}\right) & \frac{kA}{h_1} \\ \frac{kA}{h_2} & -\left(\frac{kA}{h_2} + \frac{k_w A_w}{w_t}\right) \end{bmatrix} \begin{Bmatrix} T_1 \\ T_2 \end{Bmatrix} + \begin{bmatrix} 0 \\ c_v(T_{en} - T_{ex}) \end{bmatrix} \{\dot{m}_c\} + \begin{bmatrix} c_v(T_2 - T_1) & \frac{k_w A_w}{w_t} \\ c_v(T_{cw} - T_2) & \frac{k_w A_w}{w_t} \end{bmatrix} \begin{Bmatrix} \dot{m}_t \\ T_0 \end{Bmatrix} \quad (10)$$

We can substitute T_2 for T_{ex} and linearize the governing differential equations to eliminate all bilinear terms resulting from the multiplication of $\dot{m}_t$ and $\dot{m}_c$ with the dynamic states, T_1 and T_2. This then

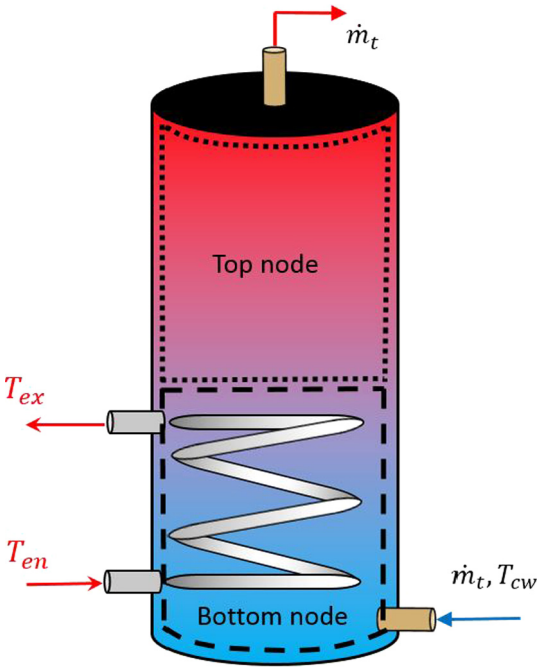

Fig. 10. Schematic for simulated case study of model-based feedback control to demonstrate modulation of coil flow rate.

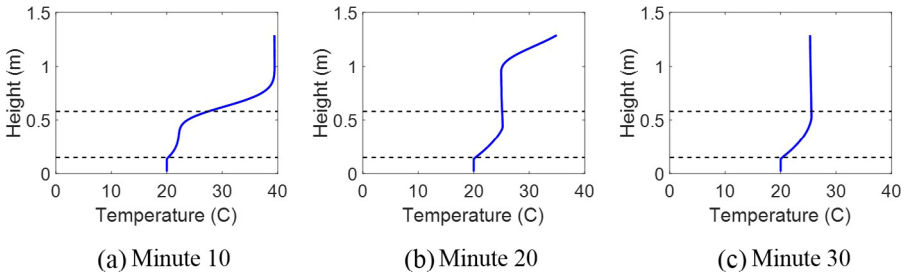

Fig. 9. Illustration of temperature evolution during 30 min simultaneous charge/discharge.

yields a linear time-invariant (LTI) state-space representation. The state derivative vector, $\{\dot{T}_1 \quad \dot{T}_2\}^T$ is augmented with a tracking state whose dynamics $\dot{\varepsilon} = T_1 - r$ are used to force the temperature of the top node to track a specified set point temperature, or reference temperature, r. In the linearized model, all states, control inputs, and disturbance inputs shown are with respect to nominal values. The resulting LTI system is given in Eq. (11).

$$\begin{Bmatrix} \frac{dT_1}{dt} \\ \frac{dT_2}{dt} \\ \frac{d\varepsilon}{dt} \end{Bmatrix} = \begin{bmatrix} -\frac{1}{m_1 c_v}\left(\frac{kA}{h_1}+\frac{k_w A_w}{w_t}+\dot{m}_t^e c_v\right) & \frac{1}{m_1 c_v}\left(\frac{kA}{h_1}+\dot{m}_t^e c_v\right) & 0 \\ \frac{1}{m_2 c_v}\left(\frac{kA}{h_2}\right) & -\frac{1}{m_2 c_v}\left(\frac{kA}{h_2}+\frac{k_w A_w}{w_t}+\dot{m}_t^e c_v + c_v \dot{m}_c^e\right) & 0 \\ 1 & 0 & 0 \end{bmatrix} \begin{Bmatrix} T_1 \\ T_2 \\ \varepsilon \end{Bmatrix} + \begin{Bmatrix} 0 \\ \frac{1}{m_2}(T_{en}-T_2^e) \\ 0 \end{Bmatrix} \{\dot{m}_c\} + \begin{bmatrix} \frac{1}{m_1}(T_2^e - T_1^e) & \frac{k_w A_w}{m_1 c_v w_t} & 0 \\ \frac{1}{m_2}(T_{cw}-T_2^e) & \frac{k_w A_w}{m_2 c_v w_t} & 0 \\ 0 & 0 & -1 \end{bmatrix} \begin{Bmatrix} \dot{m}_t \\ T_0 \\ r \end{Bmatrix} \quad (11)$$

We now consider a situation where the top node of the tank is at a temperature of 24 °C. The control objective is to first warm the top node to its set point temperature of 25 °C, and to then keep it there in the presence of a pulsed domestic hot water disturbance $\dot{m}_t$. A controller can be designed to modulate the coil flow rate, $\dot{m}_c$, to meet these objectives.

In order to modulate $\dot{m}_c$, a linear quadratic regulator (LQR) is designed [38]. LQR is a desirable controller design due to its ease in design and implementation. These controllers are perfectly suited to be used in complex applications, such as integration with a larger micro-CHP unit. LQR controllers are designed offline and provide an optimal path (in terms of some cost) to a desired state. To design the controller, a linear state-space representation is required (Eq. (11)). The synthesis of a LQR results in an optimal control law that governs system operation. This control law is given by

$$\dot{m}_c = -[K_1 \quad K_2 \quad K_3] \begin{Bmatrix} T_1 \\ T_2 \\ \varepsilon \end{Bmatrix}, \quad (12)$$

where $[K_1 \quad K_2 \quad K_3]$ is a row vector of static gains synthesized by the LQR.

The feedback controller was simulated with the linear storage tank model in MATLAB, and the results are shown in Fig. 11.

At time $t = 0$, the temperature of water in the top node (the water being discharged) is one degree below its desired set point temperature. Therefore, the commanded coil flow rate starts out high (≈0.167 kg/s). As the temperature of the tank water nears the set point, the coil flow rate decreases to transfer less heat to the tank. As the water temperature rises and actually overshoots the set point, the coil flow shuts off completely until more heat transfer is again needed to raise the water temperature and stabilize it at the set point. At $t = 10$ min the domestic water flow increases from 0.063 kg/s to 0.63 kg/s; to compensate, the coil flow rate is increased in order to return the temperature of the tank to its set point. Conversely, at $t = 20$ min, the domestic water flow drops to 0.315 kg/s Now, the coil flow rate modulates downward to avoid overcompensating for the amount of hot water being removed from the storage tank. In this manner, the simplicity of the derived model allows for effective controllers to be designed and implemented. The simple relationship between the storage tank temperature profile and the IHX coil flow rate allows for easy modulation of the flow rate to reach desired performance criteria.

In the following section, we describe a model-tuning and experimental validation procedure for the model derived in this section. We then present model tuning results for charging mode and discharging mode and validation results for simultaneous charging/discharging mode.

4. Experiments

In this section, we first describe the experimental setup used to tune and validate our control-oriented model. We then compare experimental data with data obtained from the simulation model for the three major modes of system operation: (1) charging, (2) discharging, and (3) simultaneous charging/discharging. Each of the three modes is examined both spatially and temporally. A discussion of key findings is presented.

4.1. Experimental setup

We tune and validate the simulation model using a commercially available 0.151 m^3, or 151 l, domestic hot water storage tank. The storage tank measures approximately 1.42 m in external height (1.30 m internal) with a 0.38 m approximate inner diameter and a 0.51 m outer diameter. A 0.0254 m diameter immersed coil with a fluid capacity of approximately 0.0075 m^3, or 7.5 l, is situated toward the bottom of the tank. The storage tank and IHX coil are part of an integrated micro-combined heat and power (micro-CHP) system driven by a proton exchange membrane (PEM) fuel cell. Deionized water absorbs heat from the fuel cell and is then pumped through the IHX coil for heat exchange with the storage tank water. A photo of the overall integrated micro-CHP system with the experimental storage tank, located in the Herrick Laboratories at Purdue University, is shown in Fig. 12.

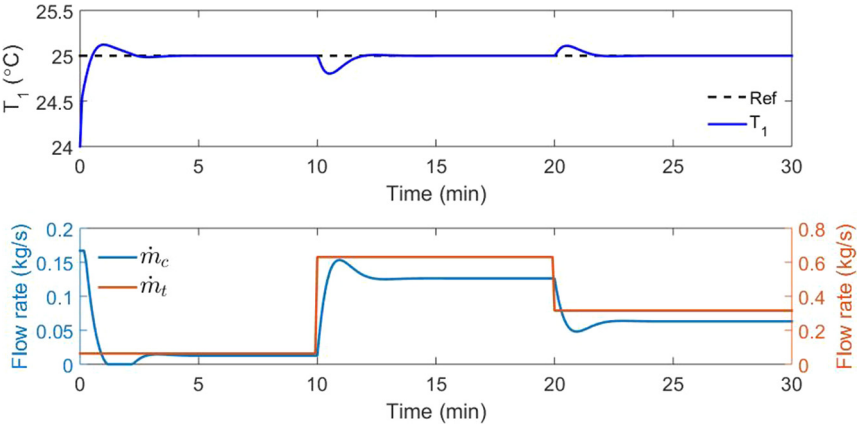

Fig. 11. Simulation results for model-based feedback control case study: at top, regulation of top node temperature to a reference value; at bottom, pulsed domestic water disturbance $\dot{m}_t$ and modulation of control variable $\dot{m}_c$ needed for regulation.

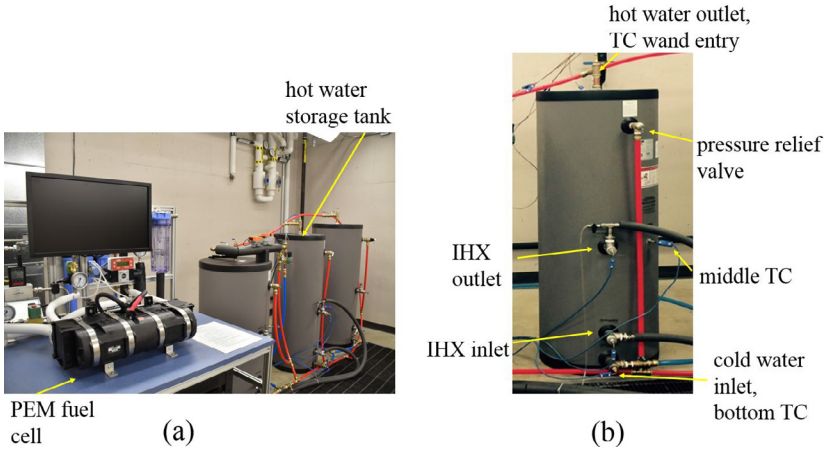

Fig. 12. Photos of experimental system. (a) integrated micro-CHP system with PEM fuel cell, (b) hot water storage tank.

There are thermocouple (TC) rods inserted horizontally into the tank at the cold water inlet and in a well located approximately halfway up the side of the tank. Additionally, a custom TC wand is inserted vertically through the hot water outlet valve at the top of the tank. The TC wand adds six experimental temperature measurements, although TC_4 is left unused in all experiments in this work. Table 3 provides the vertical distance from the bottom of the tank to all relevant valves and TCs, and Fig. 13 shows a schematic of the TC setup.

Table 3
Physical specifications for experimental data collection. The values in the height column represent the vertical distance of each respective component from the bottom of the tank. Thermocouples on the wand have positional uncertainty due to an estimated measurement of inner tank height.

Component	Height (m)
TC_{Bottom}	0.09
IHX inlet	0.15
TC_1	0.18 ± 0.05
TC_2	0.30 ± 0.05
TC_3	0.46 ± 0.05
IHX outlet	0.58
TC_{Middle}	0.60
TC_5	0.97 ± 0.05
TC_{Hot}	1.19 ± 0.05

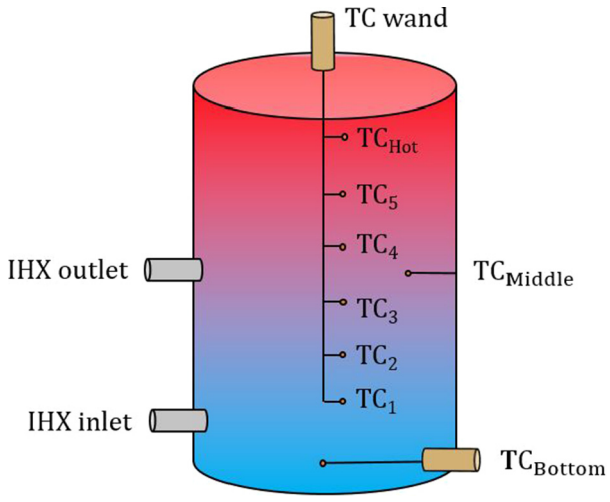

Fig. 13. Schematic of thermocouple locations used in experimental data collection.

Table 4
Specifications for instruments used in collecting temperature and flow rate data.

Device	Range	Accuracy
IHX coil flow meter	$2.51 \cdot 10^{-6}$ to $3.16 \cdot 10^{-4}$ m^3/s	$\pm 3.17 \cdot 10^{-6}$ m^3/s
Domestic flow meter	$5.01 \cdot 10^{-6}$ to $6.28 \cdot 10^{-4}$ m^3/s	$\pm 6.68 \cdot 10^{-6}$ m^3/s
Thermocouples	−250 to 350 °C	±1 °C

Each experiment is conducted in a temperature controlled room with an ambient temperature of 23 °C. In addition to the TC temperature measurements, we also record the coil inlet and outlet fluid temperatures as well as the volumetric flow rates of both the domestic hot water discharge and the IHX coil water. Data is collected at a sampling rate of approximately 0.15 s. Measurement ranges and accuracies for the flow rate and temperature measurements are shown in Table 4.

4.2. Charging mode model tuning

To tune the derived model for charging mode, the water in the tank is first allowed to reach equilibrium with the ambient environment so that an accurate picture of the temperature evolution within the tank can be captured. Hot DI water is pumped through the IHX coil at a varying volumetric flow rate in the range of $1.67 \cdot 10^{-5} - 5.01 \cdot 10^{-5}$ m^3/s, or 1–3 liters per minute (lpm). The domestic cold water inlet valve and hot water outlet valve are closed to prevent the system from entering discharge mode. Experimental data is collected over a period of two hours. The experimental coil inlet temperature and volumetric flow rate time histories are then used as inputs to the simulation model to predict the temperature evolution in the tank over a two-hour period. Fig. 14 shows a *spatial* comparison of the experimental data and the results from the model simulation. The model temperature predictions, after tuning to the values in Table 5, remain within approximately one degree of the experimental values throughout the experiment.

A major assumption in the development of the model is that the IHX coil fluid outlet temperature T_{ex} is equal to the temperature of the surrounding water at any time t. This assumption plays a major part in allowing a simple model formulation for real-time control. Fig. 15 illustrates the accuracy of the assumption.

The IHX coil outlet fluid temperature, as predicted by the tuned model, remains in close agreement with its experimental value throughout the charge mode. This indicates the heat exchanger effectiveness assumption allows accurate characterization of the charge dynamics after model tuning.

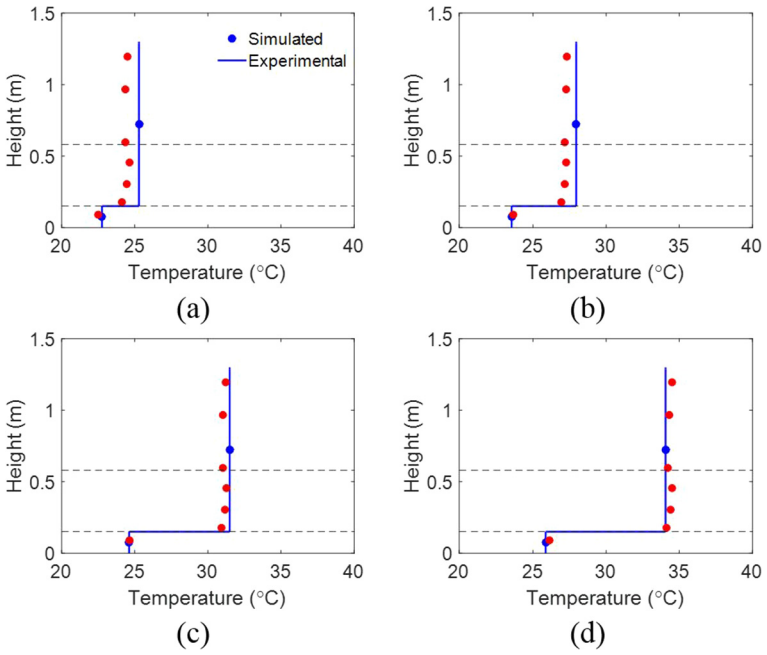

Fig. 14. Spatial temperature profile in the storage tank after (a) 30 min, (b) 60 min, (c) 90 min, and (d) 120 min. The low-order storage tank model accurately characterizes the heat addition due to the IHX coil and successfully corrects for the temperature inversion caused by the coil.

Table 5
Tuning parameter values for charge mode model-tuning. Note that s_1 remains unused during pure charge mode as there is no discharge flow.

Tuning parameter	Value
k_w	2 W mK^{-1}
k	50 W mK^{-1}
Δ	100,000

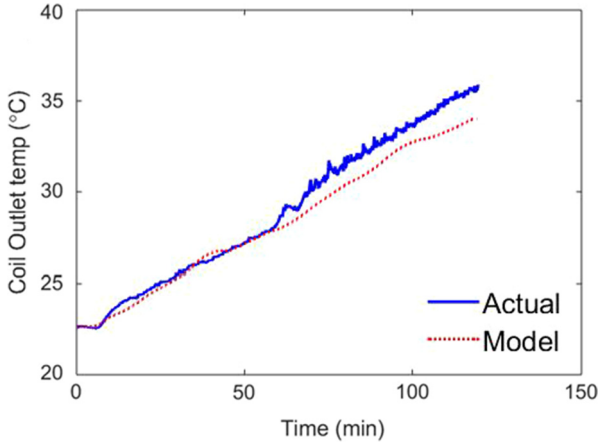

Fig. 15. Difference between experimental T_{ex} and the model prediction of T_{ex}.

The spatial tuning of the model during charging mode illustrates the ability of the IHX model to accurately predict the thermal gradient over time. While the assumptions made in deriving the algebraic IHX model neglect certain dynamics, they still enable accurate characterization of the stratification within the tank throughout charging mode. As the charge progresses, the water in and above the IHX coil region heats up uniformly, while the water below the bottom of the coil remains at a near constant temperature. The two-node charge mode model is still able to accurately capture these dynamics. To further illustrate the accuracy of the model, we compare the time histories of both simulation nodes with the nearest experimental TC (Fig. 16).

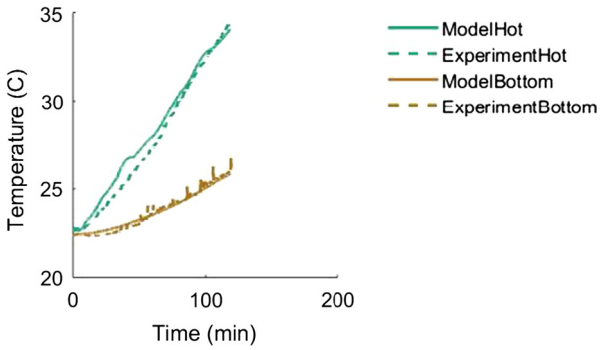

Fig. 16. Temporal tuning of charge mode. The time histories of the top–most and bottom–most experimental measurements are in agreement with the model simulation.

The temporal tuning results show each simulation node to be in good agreement with the experimental measurements, indicating that the *transient* dynamics of charge mode are accurately captured by the ideally stratified two-node model.

4.3. Discharge mode model tuning

For model tuning of the discharge mode, the storage tank is filled with domestic hot water at a temperature of approximately 50 °C. The initial temperature data is used to provide the simulation model with a matching initial profile. The inlet and outlet IHX valves are closed to prevent additional heat from being added by the coil. At the five minute mark, the domestic hot water inlet and outlet valves are opened and hot water is discharged from the top of the storage tank at a rate of approximately $1.17 \cdot 10^{-4}$ m^3/s, or approximately 7 liters per minute. The dis-

charged water is replenished by domestic cold water assumed to be at a temperature equal to that measured by the bottom TC. This assumption is based on the fact that the bottom TC is inserted into the tank directly through the cold water inlet valve.

Temperature data is recorded along with measured values of the discharge volumetric flow rate; the latter will be used as an input to the model for tuning purposes. The tuning parameters are given in Table 6.

Fig. 17 presents the spatial results for the discharge mode. Moving sequentially from Fig. 17a-f, we observe the model's ability to track the moving thermocline. Initially, cold water is pumped into the hot tank, resulting in a defined thermocline at the bottom. As more cold water replenishes the discharged hot water, the thermocline moves upward through the tank. At the end of the experiment, the tank water exists almost exclusively at the domestic cold water supply temperature. We believe the discrepancy between model and experiment at the top of the tank is likely a function of the model being overly diffusive, which will be discussed further shortly. While the model does well in predicting the temperature gradient in the tank as a function of position (spatial gradient) at discrete time instants, it is important to predict the temperature in a given node as it varies with time during the discharge mode. For example, depending on the desired performance, it could be more crucial to have accurate predictions at a certain position within the storage tank. To examine these transients, we examine the model temporally by comparing the time histories of each TC with the simulation node closest in height. These results are presented in Fig. 18.

The temporal analysis shows that the experimentally measured time histories are in general agreement with the simulation model, especially in the middle portion of the tank. The largest errors between model and experiment exist for the bottom TC and the two topmost TCs. For the bottom TC, the error is likely due to an overestimation of the inlet fluid temperature. As previously discussed, the domestic cold water inlet temperature is assumed equal to that measured by the bottom TC. Additionally, there is some discrepancy between model and experiment for the two uppermost measurements. More specifically, the model predicts slower evolving transients than is observed in the experimental data in these nodes. We believe this is again due to the model being overly diffusive, which is a function of the first-order upwind discretization scheme used in the model.

Table 6
Tuning parameter values for discharge mode model-tuning.

Tuning parameter	Value
k_w	0.25 W mK^{-1}
k	1 W mK^{-1}
Δ	100,000
s_1	0.92

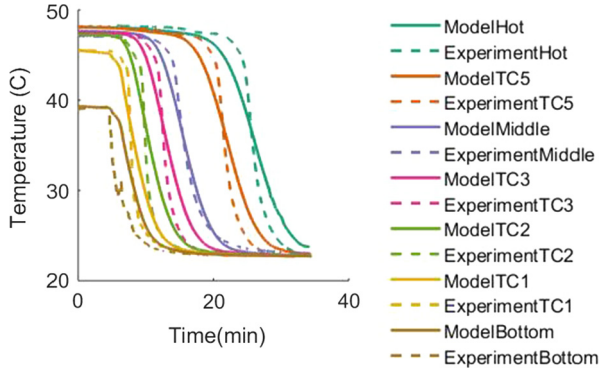

Fig. 18. Temporal analysis of discharge operation mode.

4.4. Simultaneous charge/discharge mode validation

We have shown both the model's ability to predict heat addition due to the IHX coil and heat rejection due to discharge water flow. We now present validation results for the mode in which charge and discharge are occurring simultaneously. Initially, the storage tank contains water at approximately 45 °C, and the simulation model is given a matching profile to start. We run a 45 min experiment in which domestic water flows through the tank at a rate of approximately $6.68 \cdot 10^{-5}$ m^3/s, or 4 liters per minute. Waste heat water is pumped through the IHX coil in the range of $1.67 \cdot 10^{-5} - 5.01 \cdot 10^{-5}$ m^3/s, or 1–3 liters per minute. The temperature and volumetric flow rates of both the coil inlet water and domestic cold inlet water are used as data inputs to the derived model. The tuning parameters are kept consistent with those from the discharge mode (Table 6). Spatial temperature profiles throughout the progression of the experiment are shown in Fig. 19.

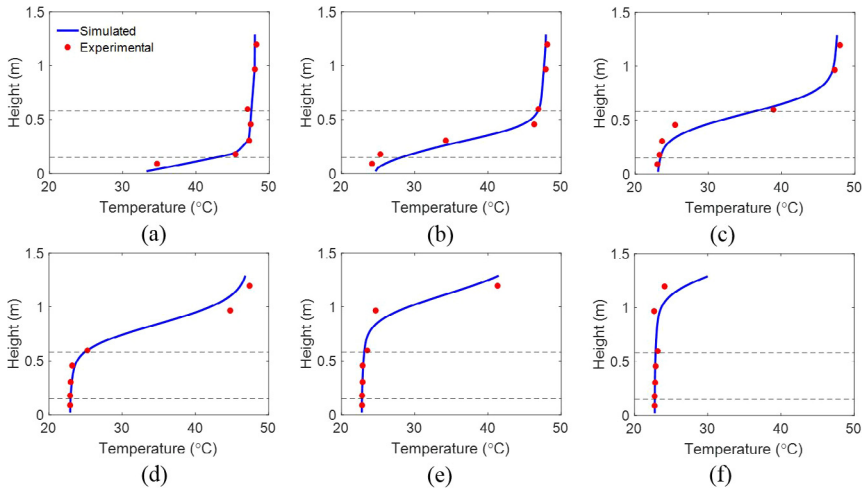

Fig. 17. Spatial temperature profile in the storage tank after (a) 5 min, (b) 10 min, (c) 15 min, (d) 20 min, (e) 25 min, and (f) 30 min. The simulation model accurately tracks the thermocline as it moves upward during discharge mode.

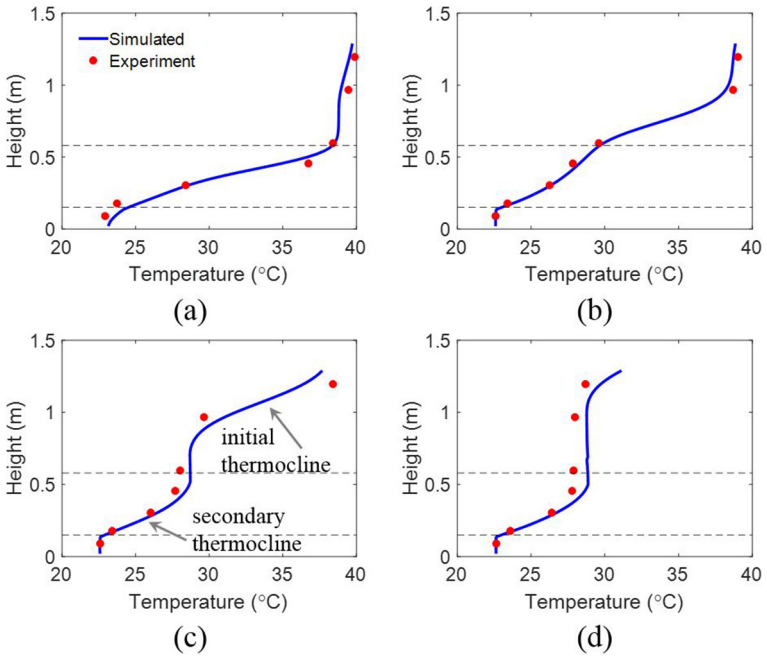

Fig. 19. Spatial temperature profile in the storage tank after (a) 10 min, (b) 20 min, (c) 30 min, and (d) 40 min. The simulation is capable of tracking both the original thermocline and the secondary thermocline that is introduced as the input cold water is heated by the IHX coil.

An initial thermocline exists (Fig. 19a) after ten minutes in the lower portion of the tank as the IHX heats the incoming cold water. In Fig. 19b, we see that the thermocline has moved upward within the tank. In Fig. 19c, a secondary thermocline has formed. As the first thermocline has moved completely out of the IHX region, a new one develops as subsequent cold water is heated by the coil. Finally, in Fig. 19d, an isothermal profile has nearly formed above the coil region. The input cold water is heated as it moves through the IHX coil region and a uniform hot temperature section exists above the top of the IHX coil.

Just as in the pure discharge mode, we also seek to conduct a temporal validation of the model (Fig. 20). Again, the time histories for each TC resemble that of the nearest simulation node. Similar to the discharge temporal validation results, the largest errors occur for the topmost and bottom-most nodes. The results in Figs. 19 and 20 illustrate the ability of the model to characterize the full system dynamics during charge/discharge mode. The model is able to simultaneously capture the heat addition dynamics due to the IHX coil and the heat rejection dynamics due to hot water discharge. The ability to accurately capture these dynamics, both spatially and temporally, will enable the use of model-based control design techniques for ultimately achieving demand response using TES systems.

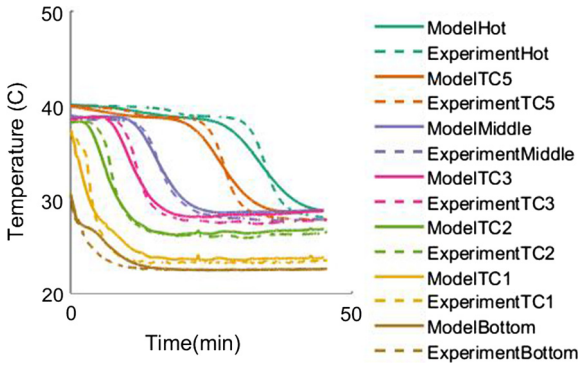

Fig. 20. Temporal validation of simultaneous charge/discharge operation mode.

4.5. Model discretization and fidelity

An important purpose of the control-oriented model is real-time simulation and model-based control design. As such, it is important to characterize the relationship between model complexity and model fidelity. To examine this, we normalize the experimental and simulated temperature data for the simultaneous charge/discharge mode based on the maximum and minimum measured temperatures (Fig. 20) and compute a root mean square error (RMSE) value for the data set. We repeat the simulation and RMSE calculation for varying degrees of model discretization ranging from five nodes to 75 nodes. The RMSE is calculated according to Eq. (13) and the results are summarized in Fig. 21.

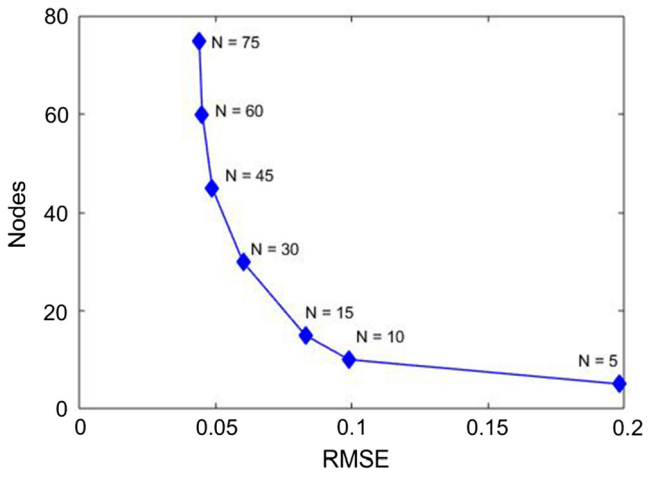

Fig. 21. The relationship between model complexity and fidelity for the simultaneous charge/discharge mode of operation. As the discretization increases, the fidelity of the model improves.

$$\mathrm{RMSE} = \frac{1}{T_{max} - T_{min}} \cdot \sqrt{\frac{\sum_{j=1}^{7}\sum_{i=1}^{n}\left(\widehat{T}_{i,j} - T_{i,j}\right)^2}{7n}} \tag{13}$$

We see that there is a definite point of diminishing return with respect to model fidelity. With excessive discretization, the resulting RMSE value does not decrease by a significant amount. Depending upon the user's needs for the model, the number of nodes can be chosen accordingly.

5. Conclusion

Currently, there remains untapped potential in both recovering and utilizing low- to medium-temperature waste heat. A major challenge is that the availability of this thermal energy may not be synchronized with its demand. Fortunately, thermal energy storage (TES) systems can be used to temporally decouple recovery of this waste heat from its utilization. However, to do so efficiently requires advanced control of the TES system which in turn requires an appropriate model of the system dynamics. In this work, we derived a control-oriented model of a sensible liquid thermal energy storage tank with a helical immersed heat exchanger (IHX) coil situated at the lower portion of the tank. We used key simplifying assumptions to develop a quasi-steady model of the IHX coil heat transfer dynamics to avoid adding any additional dynamic states to the overall simulation model. The IHX coil model is independent of heat transfer correlations and easily parameterized with respect to the flow rate of water pumped through the coil.

Through simulation, we found the derived model to run up to 1200× faster than real-time. We also demonstrated the utility of the model through a simulated case study in which an optimal feedback controller was designed and implemented to regulate the temperature of the water exiting the storage tank during simultaneous charge and discharge mode. Using a commercially available domestic hot water storage tank, we empirically tuned the control-oriented model in both charge and discharge modes. We then experimentally validated the model during simultaneous charge and discharge mode. Finally, we quantified the trade-off between model fidelity and increased control volume discretization, showing that a 60 node model yields a RMSE value under 4.5%. In future work, the control-oriented model will be used for the design and implementation of model-based energy management strategies for waste heat recovery applications.

References

[1] Waste heat recovery – technology and opportunities in U.S. industry. Technical report, BCS, incorporated; 2008.
[2] Semkov K, Mooney E, Connolly M, Adley C. Efficiency improvement through waste heat reduction. Appl Therm Eng 2014;70:716–22.
[3] Estimated U.S. energy consumption in 2015: 97.5 quads. Technical report, Lawrence Livermore National Laboratory (LLNL) flow charts; 2015. <https://flowcharts.llnl.gov/commodities/energy>.
[4] International energy outlook 2016. Technical report DOE/EIA-0484(2016), U.S. Energy Information Administration; 2016.
[5] Bindlish R. Power scheduling and real-time optimization of industrial cogeneration plants. Comput Chem Eng 2016;87:257–66.
[6] Miró L, Gasia J, Cabeza LF. Thermal energy storage (tes) for industrial waste heat (iwh) recovery: a review. Appl Energy 2016;179:284–301.
[7] Bell LE. Cooling, heating, generating power, and recovering waste heat with thermoelectric systems. Science 2008;321:1457–61.
[8] Waste Heat recovery technology assessment. Technical report, U.S. Department of Energy; 2015.
[9] Request for Information (RFI) DE-FOA-0001607 on lower grade waste heat recovery. Technical report, U.S. Department of Energy Advanced Research Projects Agency – Energy; 2016.
[10] Powell KM, Edgar TF. An adaptive-grid model for dynamic simulation of thermocline thermal energy storage systems. Energy Convers Manage 2013;76:865–73.
[11] Baeten B, Confrey T, Pecceu S, Rogiers F, Helsen L. A validated model for mixing and buoyancy in stratified hot water storage tanks for use in building energy simulations. Appl Energy 2016;172:217–29.
[12] Van Berkel J, Rindt CCM, Van Steenhoven AA. Thermocline dynamics in a thermally stratified store. Int J Heat Mass Transfer 2002;45:343–56.
[13] Van Berkel J. Mixing in thermally stratified energy stores. Solar Energy 1996;58:203–11.
[14] Hahne E, Chen Y. Numerical study of flow and heat transfer characteristics in hot water stores. Solar Energy 1998;64:9–18.
[15] Shin M-S, Kim H-S, Jang D-S, Lee S-N, Lee Y-S, Yoon H-G. Numerical and experimental study on the design of a stratified thermal storage system. Appl Therm Eng 2004;24:17–27.
[16] Han Y, Wang R, Dai Y. Thermal stratification within the water tank. Renew Sustain Energy Rev 2009;13:1014–26.
[17] Shah LJ, Furbo S. Entrance effects in solar storage tanks. Solar Energy 2003;75:337–48.
[18] Cònsul R, Rodríguez I, Pérez-Segarra C, Soria M. Virtual prototyping of storage tanks by means of three-dimensional CFD and heat transfer numerical simulations. Solar Energy 2004;77:179–91.
[19] Campos Celador A, Odriozola M, Sala J. Implications of the modelling of stratified hot water storage tanks in the simulation of CHP plants. Energy Convers Manage 2011;52:3018–26.
[20] Kleinbach E, Beckman W, Klein S. Performance study of one-dimensional models for stratified thermal storage tanks. Solar Energy 1993;50:155–66.
[21] Zurigat YH, Maloney KJ, Ghajar AJ. A comparison study of one-dimensional models for stratified thermal storage tanks. J Solar Energy Eng 1989;111:204–10.
[22] Arslan M, Igci AA. Thermal performance of a vertical solar hot water storage tank with a mantle heat exchanger depending on the discharging operation parameters. Solar Energy 2015;116:184–204.
[23] Soo Too Y, Morrison G, Behnia M. Performance of solar water heaters with narrow mantle heat exchangers. Solar Energy 2009;83:350–62.
[24] Huang J, Pu S, Gao W, Que Y. Experimental investigation on thermal performance of thermosyphon flat-plate solar water heater with a mantle heat exchanger. Energy 2010;35:3563–8.
[25] Cadafalch J, Carbonell D, Consul R, Ruiz R. Modelling of storage tanks with immersed heat exchangers. Solar Energy 2015;112:154–62.
[26] Farrington R, Bingham C. Testing and analysis of load-side immersed heat exchangers for solar domestic hot water systems. U.S. Department of Energy, Solar Energy Research Institute; 1987.
[27] Logie WR, Frank E. A transient immersed coil heat exchanger model. J Solar Energy Eng 2013;135:041006.
[28] Newton BJ. Modeling of solar storage tanks. Ph.D. thesis, University of Wisconsin-Madison; 1995.
[29] Mates RE. Model for an immersed, collector side heat exchanger. Ph.D. thesis, University of Wisconsin-Madison; 1987.
[30] Mather DW, Hollands KGT, Wright JL. Single-and multi-tank energy storage for solar heating systems: fundamentals. Solar Energy 2002;73:3–13.
[31] Mote R, Probert SD, Nevrala D. The performance of a coiled finned-tube heat-exchanger submerged in a hot-water store: the effect of the exchanger's orientation. Appl Energy 1991;38:1–19.
[32] Prabhanjan DG, Rennie TJ, Vijaya Raghavan G. Natural convection heat transfer from helical coiled tubes. Int J Therm Sci 2004;43:359–65.
[33] Xin RC, Ebadian MA. Natural convection heat transfer from helicoidal pipes. J Thermophys Heat Transfer 1996;10:297–302.
[34] Reindl DT, Beckman WA, Mitchell JW. Transient natural convection in enclosures with application to solar thermal storage tanks. J Solar Energy Eng 1992;114:175–81.
[35] Ali ME. Experimental investigation of natural convection from vertical helical coiled tubes. Int J Heat Mass Transfer 1994;37:665–71.
[36] Haltiwanger JF, Davidson JH. Discharge of a thermal storage tank using an immersed heat exchanger with an annular baffle. Solar Energy 2009;83:193–201.
[37] Su Y, Davidson JH. Natural convective flow and heat transfer in a collector storage with an immersed heat exchanger: numerical study. J Solar Energy Eng 2005;127:324.
[38] Bryson A. Applied optimal control: optimization, estimation and control. CRC Press; 1975.